Tight-binding molecular dynamics simulations of radiation-induced fragmentation of C_{60}

Lóránd Horváth and Titus A. Beu*
Faculty of Physics, University "Babeş-Bolyai", 400084 Cluj-Napoca, Romania
(Received 24 August 2007; revised manuscript received 14 November 2007; published 4 February 2008)

The fragmentation of the C_{60} fullerene was investigated using tight-binding molecular dynamics simulations based on the parametrization of Papaconstantopoulos *et al.* [MRS Symposia Proceedings No. 491 (Materials Research Society, Pittsburgh, 1998), p. 221]. Averaged fragment size distributions over random sets of initial configurations were obtained from simulations of radiation-induced fragmentation in the 50–500 eV excitation energy range. The excitation caused by the radiation was simulated simply by ascribing suddenly random velocities to each atom of the fullerene cage. For low excitation energies, the size distributions are peaked for dimers (reflecting a preferential C_2 emission) and a bimodal size dependence characterizes the distributions of the complementary small and large fragments. For high excitation energies, predominantly multifragmentation occurs, but a genuine power-law dependence of small fragments is not yet observable. A phase transition is found for rather low excitation energies (100–120 eV).

DOI: 10.1103/PhysRevB.77.075102 PACS number(s): 71.15.Mb, 71.20.Tx

I. INTRODUCTION

Collision-induced dissociation is a powerful technique to investigate the fullerene fragmentation process.[2] The fragmentation of fullerene ions induced by atomic and molecular targets has been widely studied since macroscopic amounts of fullerenes were first made available. The impact with various projectiles (photons, electrons, atoms or molecules, ions, or other fullerenes) reveals the fact that fragmentation can occur via different channels, depending on the projectile type and its impact energy.[2,3] The possible processes were found to be (a) evaporation of light, neutral, even numbered C_{2n} clusters, (b) asymmetric dissociation (fission) into heavy and light (neutral or charged) fragments much smaller than C_{60}, and (c) multifragmentation into several light fragments. The detection of fragments resulting from collision experiments is usually performed using time-of-flight (TOF) spectrometers.[3–5]

The first systematic study of radiation-induced fullerene fragmentation was done by O'Brien *et al.* using nanosecond laser pulses, and the primary channel of photodissociation was found to be the loss of neutral C_2 or C_3 units.[6]

Full first-principles molecular dynamics (MD) simulations of electronic, energetic, and vibrational properties of large carbon nanostructures (such as fullerene polymers or carbon nanotubes) are still not tractable on many up-to-date computers. Therefore, there is an obvious need for alternative methods involving less computational effort, but preserving a comparable level of accuracy. Valuable options are tight-binding (TB) approaches, such as the *a priori* theory based on universal parameters of Harrison,[7,8] which can be viewed as a simplified two-center-oriented *ab initio* method, where the properties of the system are calculated from a parametrized representation of the Kohn-Sham equation.

Early orthogonal tight-binding molecular dynamics (TBMD) simulations of disintegration and formation of C_{60} have been carried out by Wang *et al.*,[9] providing, however, due to the very large time step used (0.7 fs), basically qualitative results. One of the main findings was that the fullerene is stable against spontaneous disintegration below 5000 K. At 6000 K, the fragmentation is predicted to occur after several picoseconds.

Using an empirical TB total-energy approach, Kim *et al.* have reported molecular dynamics simulations of fragmentation[10] and melting[11] of several carbon fullerenes. They focused primarily on calculating the heat capacities, binding energies, and pair correlation functions in terms of temperature. With increasing temperature, the heat capacity and binding energy of a C_{60} molecule were found to increase up to 3000 K and then decrease, saturating at some constant value around 5000 K. Their analysis revealed structural changes in the fullerene cage between 3000 and 4000 K, with bonds starting to break at approximately 5000 K. Once the bonds start breaking, the fragmentation process is estimated to occur very rapidly, within 1 ps. The calculated fragmentation temperature (5400 K) is close to the observed boiling point of graphite (5100 K).[11]

Recently, density-functional-based tight-binding simulations of the response of C_{60} and carbon chains to laser pulses have been performed by Torralva *et al.*[12] By analyzing individual molecular dynamics trajectories, the calculations have evidenced that the excitation of the pentagonal-pinch mode is dominant at low laser fluencies, the breathing mode is dominant at high fluencies, and dimers are preferentially emitted during photofragmentation (however, without providing a detailed analysis of the fragmentation statistics).

The elaborate and yet conveniently implementable parametrization scheme of Papaconstantopoulos *et al.*[1] has proved to describe structural properties of carbon systems accurately (comparable to first-principles methods), allowing, in the framework of the TB theory of Harrison, for larger systems to be simulated than with other approaches available. Over the past decade, we have successfully employed this parametrization for describing structural and vibrational properties of the C_{36}, C_{60}, and C_{70} fullerenes and of their polymers.[13–16]

The present paper reports simulation results of radiation-induced C_{60} fullerene fragmentation by means of the mentioned TBMD method. The effect of the radiation was simulated in a simple way by merely ascribing adiabatically random velocities to each atom of the fullerene cage. As

 ©2008 The American Physical Society

compared to previous TB calculations, the strong points of our approach stem from the fact that it is more accurate, being based on a more recent and elaborate nonorthogonal parametrization resulted from fits to experiments and *ab initio* data, still allowing for intensive calculations on large systems to be performed in a reasonable amount of time and for a full ensemble-statistical analysis to be carried out.

Excitation energy dependent fragment size statistics has been simulated and analyzed. Specifically, fragment size distributions, average fragment sizes and number of fragments per trajectory, average and overall minimum and/or maximum fragment sizes, binding energies, and relative and/or cumulative fragmentation probabilities have been calculated. While for high excitation energies, predominantly multifragmentation occurs and a tendency to develop a power-law distribution of the small fragments appears, for low excitation energies, the fragment size distributions are peaked at sizes $n=2$ or 3. Noteworthy is a phase transition which is found in the 100–120 eV energy range. As a consequence of the simple representation of the excitation due to the radiation, possible rapid fragmentation that could take place as a result of electronic excitation (including ionization) over time scales shorter than 0.5–2.5 ps is disregarded. The results are compared with experimental time-of-flight fragmentation distributions and are in good agreement with similar theoretical studies.[2,4,5,17]

II. NONORTHOGONAL TIGHT-BINDING MOLECULAR DYNAMICS

In tight-binding total-energy (TBTE) models based on the Kohn-Sham *ansatz* to density-functional theory,[18] the total energy of the system can be expressed as the sum of the "band structure energy" (sum of occupied one-electron energies) and a short-range repulsive pair potential (accounting for the corrections to the single-particle picture):

$$E_{\mathrm{tot}}(\{\mathbf{R}_J\}) = \sum_{k=1}^{n_{\mathrm{occ}}} n_k \varepsilon_k(\{\mathbf{R}_J\}) + \sum_{J<K} V_{\mathrm{rep}}(|\mathbf{R}_J - \mathbf{R}_K|). \quad (1)$$

The one-electron energies ε_k are eigenvalues of the characteristic equation

$$(\mathbf{H} - \varepsilon_k \mathbf{S})\mathbf{C}^k = 0, \quad (2)$$

where the Hamiltonian matrix $\mathbf{H}$ and the overlap matrix $\mathbf{S}$ are expressed relative to some nonorthogonal set of atom-centered orbitals. $\mathbf{C}^k$ is the eigenvector corresponding to eigenvalue ε_k.

Most TBTE models use a parametrized pair potential to represent the repulsive contribution to the total energy. However, the Kohn-Sham formulation allows the eigenvalues to be shifted by an arbitrary constant. The TB parametrization of Papaconstantopoulos *et al.*,[1] used throughout in this work, eliminates the pair potential by choosing the arbitrary zero for each band structure such that the total energy is given solely by the sum of the (shifted) one-electron energies.

The forces acting on the atoms are related to the gradients of the total energy at the atom sites and, according to Eqs. (1) (without repulsive term) and (2), they are formally

$$\mathbf{F}_I = -\frac{\partial E_{\mathrm{tot}}}{\partial \mathbf{R}_I} = -\sum_{k=1}^{n_{\mathrm{occ}}} \frac{n_k}{\mathbf{C}^{k\dagger}\mathbf{S}\mathbf{C}^k} \mathbf{C}^{k\dagger}\left(\frac{\partial \mathbf{H}}{\partial \mathbf{R}_I} - \varepsilon_k \frac{\partial \mathbf{S}}{\partial \mathbf{R}_I}\right)\mathbf{C}^k. \quad (3)$$

Within the parametrization considered, they can be expressed analytically, this being an essential advantage with a view to tractable large-scale MD simulations.

Within a conventional orthogonal TB formalism, the bond orbitals for the tetrahedral structure are constructed from sp^3 hybrids. The use of sp^3 bonding for fullerenes is justified by the fact that the nominal sp^2 bonding between adjacent carbon atoms actually occurs on a curved surface, which leads to some admixture of sp^3 bonding. The total number of electrons considered for a molecule composed of N atoms is $n=4N$. The corresponding number of occupied one-electron states is $n_{occ}=n/2$, while the occupation number is $n_k=2$. The $(4N)\times(4N)$ Hamiltonian matrix for the system of valence electrons is consequently composed of 4×4 blocks corresponding to the coupling between the s, p_x, p_y, and p_z orbitals of the involved atoms:

$$\mathbf{H} = \begin{bmatrix} \ddots & \vdots & & \vdots & & \vdots & & & \vdots & \\ \cdots & h_s^I & 0 & 0 & 0 & \cdots & H_{ss}^{IJ} & H_{sx}^{IJ} & H_{sy}^{IJ} & H_{sz}^{IJ} & \cdots \\ & 0 & h_p^I & 0 & 0 & & -H_{sx}^{IJ} & H_{xx}^{IJ} & H_{xy}^{IJ} & H_{xz}^{IJ} & \\ & 0 & 0 & h_p^I & 0 & & -H_{sy}^{IJ} & H_{xy}^{IJ} & H_{yy}^{IJ} & H_{yz}^{IJ} & \\ \cdots & 0 & 0 & 0 & h_p^I & \cdots & -H_{sz}^{IJ} & H_{xz}^{IJ} & H_{yz}^{IJ} & H_{zz}^{IJ} & \cdots \\ & \vdots & & \vdots & \ddots & & \vdots & & & \vdots & \end{bmatrix}.$$

The diagonal *on-site* elements h_l^I ($l=s$ or p) can be assigned the simplified interpretation of atomic energies, but should generally be allowed to vary according to the local environment of each atom. For the Hamiltonian matrix elements of the nondiagonal block (I,J), the Slater-Koster form is usually considered.[19] In terms of bond direction cosines (γ_x^{IJ}, γ_y^{IJ}, and γ_z^{IJ}) and two-center *hopping parameters* ($H_{ss\sigma}$, $H_{sp\sigma}$, $H_{pp\sigma}$, and $H_{pp\pi}$), the relevant elements are expressed as

$$H_{ss}^{IJ} = H_{ss\sigma}^{IJ},$$

$$H_{sx}^{IJ} = \gamma_x^{IJ} H_{sp\sigma}^{IJ},$$

$$H_{xy}^{IJ} = \gamma_x^{IJ}\gamma_y^{IJ}(H_{pp\sigma}^{IJ} - H_{pp\pi}^{IJ}) + H_{pp\sigma}\delta_{xy}, \quad (4)$$

the remaining ones resulting from straightforward permutations of indices x, y, and z. Here, $\delta_{\alpha\beta}$ is the Kronecker symbol.

In a *nonorthogonal* TB formulation, except for the unitary diagonal, the block structure of the overlap matrix $\mathbf{S}$ is similar to the one of the Hamiltonian.

The TB parametrization of Papaconstantopoulos *et al.*[1] describes the environment of each atom of the system by a pseudoatomic density,

$$\rho_I = \sum_{J\neq I}^{N} \exp(-\lambda^2 R_{IJ}) f(R_{IJ}),$$

which depends exponentially on the distances to all neighbors and features a cutoff function:

$$f(R) = \frac{1}{1 + \exp[(R - R_c)/\Delta]}.$$

The particular parameters employed for carbon are $R_c = 10.5a_0$ and $\Delta = 0.5a_0$ (a_0 is the Bohr radius).

The on-site (diagonal) Hamiltonian elements are parametrized in terms of the local pseudoatomic density by

$$h_l^I = \alpha_l + \beta_l \rho_I^{2/3} + \gamma_l \rho_I^{4/3} + \chi_l \rho_I^2,$$

where $l = s$ and p. The two-center Slater-Koster[19] hopping terms are defined as polynomials with an exponential cutoff ($\mu = \sigma$ and π):

$$H_{ll'\mu}(R) = (a_{ll'\mu} + b_{ll'\mu} R + c_{ll'\mu} R^2)\exp(-d_{ll'\mu}^2 R) f(R),$$

$$S_{ll'\mu}(R) = (\delta_{ll'} + p_{ll'\mu} R + q_{ll'\mu} R^2 + r_{ll'\mu} R^3)\exp(-s_{ll'\mu}^2 R) f(R).$$

The partial derivatives of the two-center Slater-Koster terms occurring in the analytical expressions of the forces acting on the atoms [Eq. (3)] can be cast under the form

$$\frac{\partial H_{ll'\mu}(R)}{\partial R} = (b_{ll'\mu} + 2c_{ll'\mu} R)\exp(-d_{ll'\mu}^2 R) f(R) + \left[\frac{f'(R)}{f(R)} - d_{ll'\mu}^2\right] H_{ll'\mu}(R),$$

$$\frac{\partial S_{ll'\mu}(R)}{\partial R} = (p_{ll'\mu} + 2q_{ll'\mu} R + 3r_{ll'\mu} R^2)\exp(-s_{ll'\mu}^2 R) f(R) + \left[\frac{f'(R)}{f(R)} - s_{ll'\mu}^2\right] S_{ll'\mu}(R).$$

This TB parametrization considers each carbon atom to be permanently surrounded by its four valence electrons, maintaining the system and the resulted fragments electrically neutral. The simulated fragment size distributions may differ from the experimental distributions yielded by TOF spectrometers, since the latter are generally averaged both over electrically neutral and charged fragments.

III. SIMULATION DETAILS

The equilibrium geometry of the C_{60} fullerene used in our simulations was obtained by simulated annealing embedded in molecular dynamics based on the above TB framework.[13] The bond lengths obtained are 1.37 and 1.45 Å for the double and single bonds, respectively, underestimating by less than 2.5% the experimental NMR data[20] and first-principles density-functional calculation results from the literature.[21]

The excitation mechanism leading to fragmentation was chosen of extreme simplicity, avoiding artifacts which might have arisen from particular radiation inputs and, thus, preserving the generality of the results. Concretely, all atoms acquire initially random velocities, normalized according to the temperature, such that the corresponding total kinetic energy of the system amounts to the desired excitation energy. The excitation is carried out in the center-of-mass system of the initial fullerene cage, thus not affecting energy equipartition. The simple approximation of adiabatic energy transfer is justified by the relatively long typical fragmentation times (around 0.5–2.5 ps), which significantly exceed the femtosecond pulses used in laser-induced fragmentation experiments.[22,23] Obviously, due to this simple representation of the excitation, possible rapid fragmentation that could take place as a result of electronic excitation (including ionization) over time scales shorter than 0.5–2.5 ps is disregarded. Equally, the excitation of individual vibrational normal modes was not explicitly considered, since the ensemble averaging makes such detailed excitation less relevant.

The excitation energy is an appropriate reference quantity, because it allows our results to be compared with those obtained from experimental fragmentations using particles (electrons or ions), in which the so-called deposited energy can actually be measured.[4] The employed excitation energies were taken in the interval 50–500 eV. In terms of binding energy per molecule, these energies correspond to $0.083E_{\text{bind}}$–$0.83E_{\text{bind}}$ or to the 3200–32 000 K temperature range. Since the excitation energy is distributed between translational and rotational degrees of freedom of the fragments, roughly twice the total binding energy (approximately 600 eV) would be needed in order to fully dissociate the fullerene.

At the end of each trajectory, the individual fragments were identified by a recursive labeling algorithm, which essentially extends the fragments gradually by atoms which lie within a given cutoff distance. Each new member atom of a fragment becomes, in turn, the origin of a new search, avoiding, however, double counting of atoms reached along different search paths. The cutoff was set to 2 Å, which is approximately 50% above the average bond length of the initial C_{60} fullerene. Each fragmentation trajectory was propagated at constant energy until a stopping criterion was satisfied, requiring that all atoms maintain their belonging to a fragment over the last 0.25 ps, which is roughly 10% of the maximum duration considered for a trajectory. In order to reflect the statistical nature of the process, an ensemble of 200 C_{60} molecules was individually fragmented for selected excitations in the mentioned range. For each energy value, ensemble-averaged fragment size distributions were then calculated by summing up the profiles from the individual trajectories and normalizing the result to the ensemble-cumulated number of fragments. Obviously, scattering and potential recombination of fragments resulted from simultaneous fragmentations of multiple C_{60} cages have not been taken into account. However, for the typical concentrations in the experimental C_{60} beams, the cross sections of such events are expected to be low.[23]

The velocities of the individual carbon atoms strongly depend on the excitation energy, affecting the accuracy of the propagation along the trajectory. In order to preserve the same relative degree of accuracy of the total energy (10^{-3}), for each excitation energy a different but constant time step was employed, linearly decreasing from 0.25 fs for 50 eV to 0.025 fs for 500 eV.

IV. RESULTS AND DISCUSSION

The fragment size distributions for some representative excitation energies are plotted in Fig. 1. The distributions

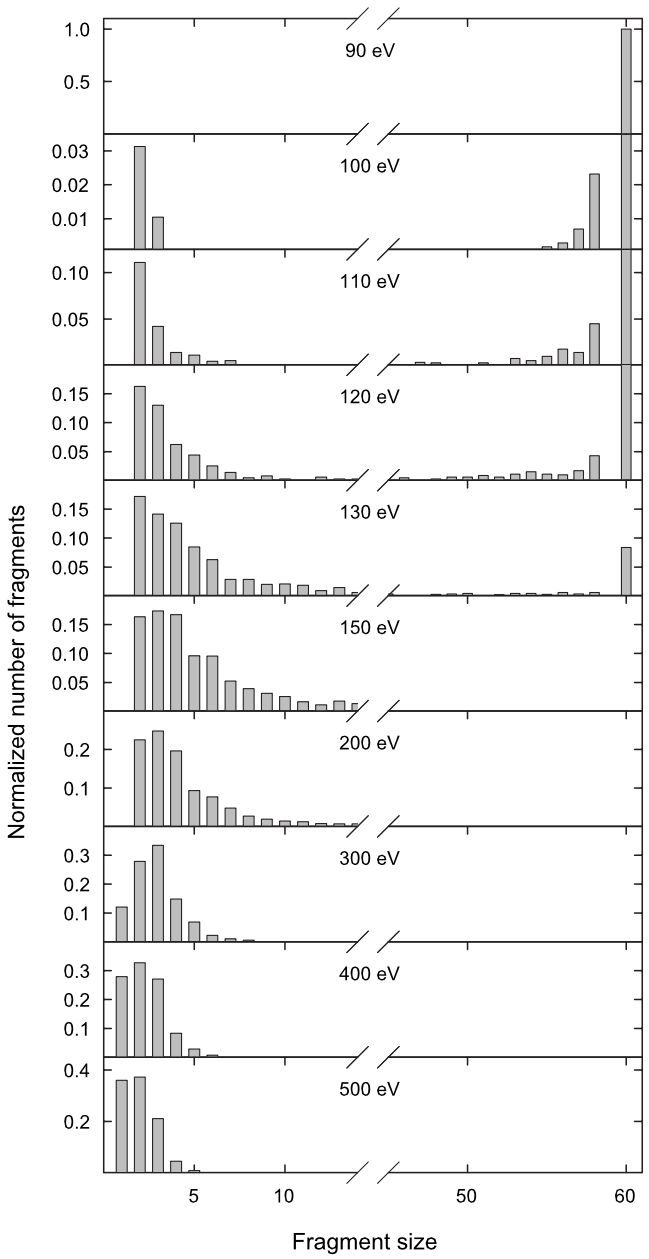

FIG. 1. Normalized number of fragments for selected excitation energies. The fragmentation is characterized by U-shaped and bimodal distributions for low energies, and by power laws for very high energies and small fragment sizes.

show a gradual shift of the maximum from large fragment sizes to smaller ones, and their U shape for relatively small energies (<150 eV) is also apparent. As speculated abundantly in the literature, these distributions appear to be similar in their U shape with those obtained in fragmentation experiments implying atomic projectiles (C_x^{q+}, H_x^+, Si^{q+}, Xe^+, and O^{q-}).[4,24–26]

There are several significant findings which result from our simulations. First, the fragmentation of the fullerene occurs roughly at excitation energies larger than 95 eV (approximately 6000 K), in very good agreement with values obtained in previous simulations of fullerene fragmentation and melting, performed by Kim *et al.*[10,11] For lower energies, the cage remains stable over a very long period of time, only a slight deformation being noticeable. Second, for excitation energies up to 500 eV, the fragment size distributions are not peaked at $n=1$ (single C atoms), as one might expect for a power law, but at higher sizes ($n=2$ or 3). Third, the contribution of the monomers increases more rapidly with the excitation energy than those of the larger fragment sizes (dimers and trimers).

Itoh *et al.*[24,27] emphasized that, provided the excitation energy is large enough, the small fragment distributions follow an $n^{-\lambda}$ power law.[4] LeBrun *et al.*[25] have measured an inclusive TOF spectrum (summed over the impact parameter) of charged fragments produced in collisions of 625 MeV Xe^{35+} ions with C_{60} targets. They observed a U-shaped fragment mass distribution which compared fairly with a bond-percolation calculation. In particular, both experiment and calculation found that the light fragment distribution follows a power-law pattern. As mentioned by Bauer,[28] the λ exponent varies amply from 0.08 to 1.8 when increasing the deposited energy.

Schlathölter *et al.*[26] found a dependence of the small fragment size distributions on the charge of equivelocity O^{q+} projectiles. For small q values (in particular, for $q=1$), their data are not peaked at $n=1$, as required for a power law, but, similar to our results, at $n=2-5$. On the contrary, for larger ionization states ($q=6$ and 7), the distributions gradually peak at $n=1$, suggesting a power law.

In Fig. 1, the gradual evolution of the *small* fragment distributions from a U shape toward a power law with increasing excitation energy is visible. For energies in the interval of 95–150 eV, the distributions peak at $n=2$. However, for intermediate energies (150–370 eV), the most probable and stable fragment was found to be C_3.

In the excitation energy range of 95–150 eV, the bimodal size dependences found for *large* fragments (at $n=54$, 56, and 58) provide hints for the successive evaporation process of C_2 units. Obviously, for higher excitation energies, fragmentation proceeds according to a different pattern—no intermediate large fragments are produced, but directly small ones. From the point of view of successive C_2 cleavage, the small and large regions of the distributions appear to be complementary. In fact, experimentally, it is well established that C_{60} should fragment with the emission of even numbered clusters.[23] The preferential dimer cleavage resulted also from the analysis of individual fragmentation trajectories in the simulations of Torralva *et al.* (in which both the initial C_{60} molecule and the fragments are electrically neutral).[12]

In addition to the usual size distribution functions, we also compare relative size distribution probabilities. In particular, the behavior of small-sized fragments is eloquent. In Fig. 2, the fragmentation probabilities for fragments up to $n=4$ are plotted against the excitation energy. The fragmentation probabilities for different fragment sizes show quite different trends. The monomer and dimer probabilities monotonously increase with the excitation energy, while for trimers and tetramers, maxima around 300 and 200 eV, respectively, are found. This implies that for very high excitation energies, the molecule is fragmented into very small fragments, mainly C_1

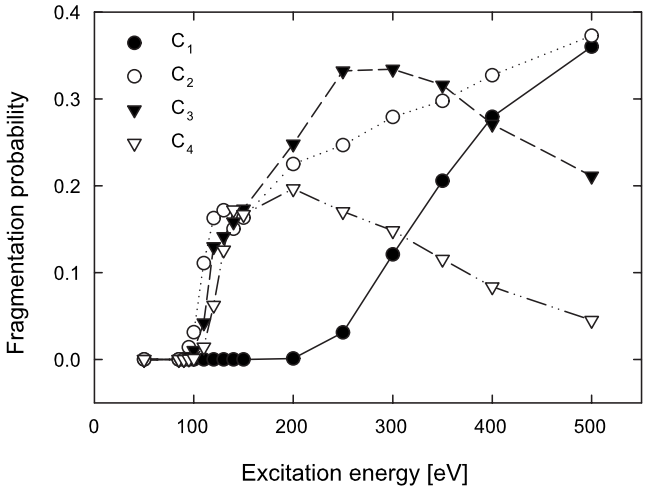

FIG. 2. Comparison of fragmentation probabilities as functions of excitation energy for small fragments ($n=1-4$). Probabilities increase faster for monomers than for other fragments.

and C_2. It is expected that for energies higher than 1200 eV, the fullerene directly disintegrates into individual carbon atoms.

Relative fragmentation probabilities of small fragments are presented in Fig. 3. Except for C_1/C_2, showing a monotonous increase, the relative probabilities exhibit a minimum (particularly sharp for C_3/C_4) in the 100–300 eV energy range. Even though the monotonous increase of the C_1/C_2 ratio suggests a gradual domination of the monomers at very high energies, within the considered energy range, a clear power-law distribution is not yet observed. Recent fragmentation results obtained by Rentenier *et al.*[4] in collision experiments of C_{60} with light charged projectiles for excitation energies similar to ours confirm that neither a U shape, intuitively expected in soft collisions (low excitation energies), nor a pure power law in hard collisions (large excitation energies) is reached, the distributions being never peaked at $n=1$.

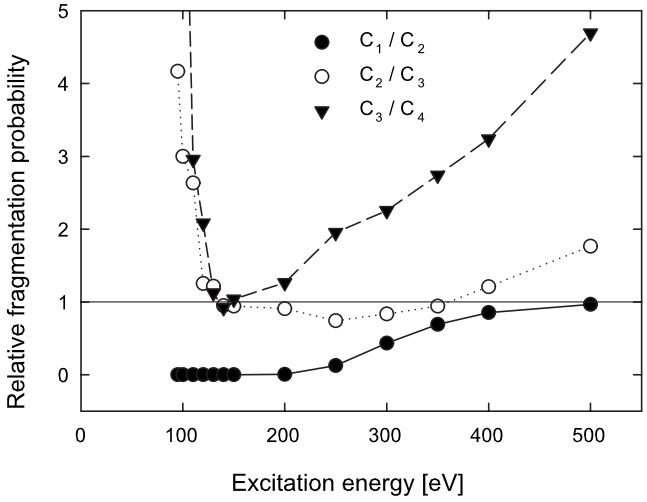

FIG. 3. Relative fragmentation probabilities for small-sized fragments as function of the excitation energy.

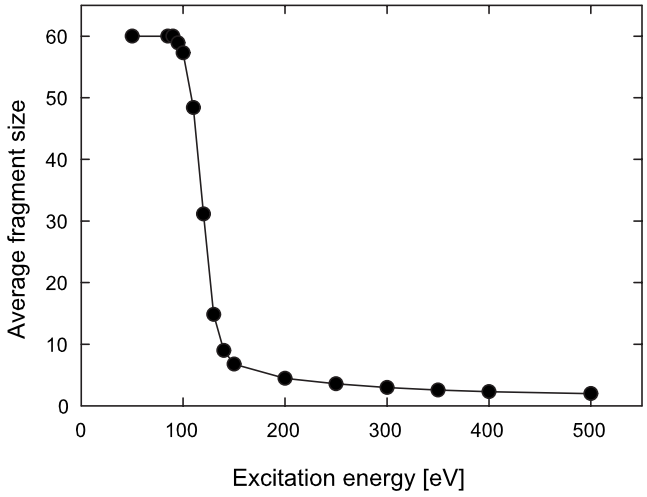

FIG. 4. The average fragment size shows its steepest decrease in the excitation energy interval of 100–120 eV, indicating a certain type of phase transition.

Various additional characteristic quantities were defined and studied as functions of the excitation energy. The average fragment size (Fig. 4) was defined as the cumulative number of atoms divided by the ensemble-cumulated number of fragments corresponding to a given excitation energy. The average minimum (maximum) fragment size for a given excitation energy was defined as the ensemble-cumulated smallest (largest) fragment size in fragmenting trajectories divided by the ensemble-cumulated number of fragmenting trajectories, and is depicted in Fig. 5. Interestingly, the average fragment size (Fig. 4) does not turn out to be barely the

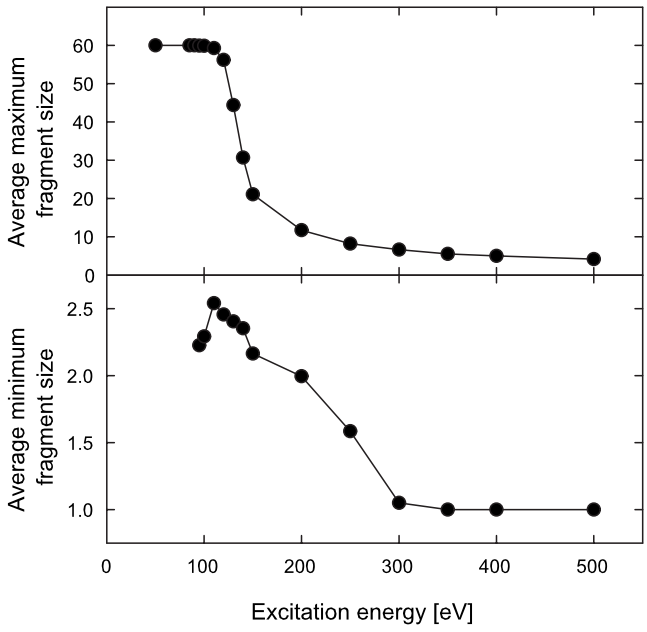

FIG. 5. Average minimum and maximum fragment sizes plotted against the excitation energy. The minimum fragment size exhibits a distinctive peak at approximately 110 eV, indicating a special energy interval for the fullerene's stability.

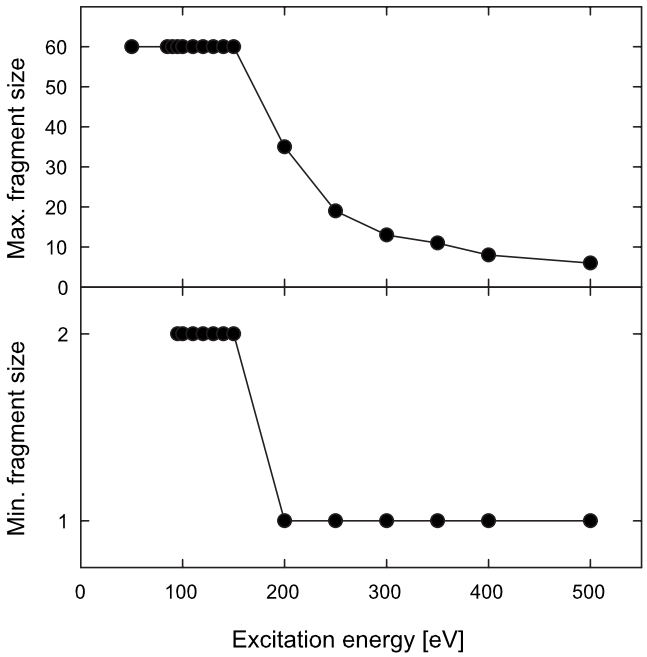

FIG. 6. Overall minimum maximum fragment size plotted against the excitation energy. A considerable ratio of fullerenes remains unfragmented for energies up to 150 eV. The continuous lines are just a visual aid.

average of the average minimum or maximum fragment sizes (Fig. 5).

The average maximum fragment size behaves similarly to the average fragment size distribution. In contrast, the average minimum fragment size distribution peaks in the 100–120 eV excitation energy range. This particular energy interval is associated with a certain type of phase transition, which is apparent in each simulated distribution.

The overall minimum (maximum) fragment size was defined as the smallest (largest) fragment found in the whole trajectory ensemble for a particular excitation energy (Fig. 6). For the simulation time considered (2.5 ps), the overall *maximum* fragment size (upper panel) remains 60 for excitation energies below 150 eV, since there are trajectories which do not result in fragmentation at all. Longer simulation times might possibly yield a slightly lower energy threshold for the fragmentation onset. The overall *minimum* fragment size profile is also significant, since the *dimer* (and not the monomer, as expected for a power law) is found to be the most probable fragment for energies up to 150 eV, while for higher energies, at least one monomer is generated.

For small excitation energies, no trajectories result in monomers, the bimodal behavior of the large fragment distributions being in fair agreement with experimental results[2,4,24,27] (see Fig. 2 of Ehlich *et al.*[29]) and other tight-binding molecular dynamics simulations.[9,30] This once more confirms, like our previous publications,[13–16] the appropriateness of the employed TB parametrization of Papaconstantopoulos *et al.*[1] for a wide range of dynamic processes involving carbon nanostructures.

In the literature, the commonly accepted explanation for the bimodal fragment distribution is given in terms of random successive C_2 evaporation processes down to an unstable fragment of about half the initial fullerene size (which eventually breaks apart) or by a cage cleavage in which large fragments are emitted.[2] Our simulations confirm the commonly accepted picture that for low excitation energies or slowly evolving fragmentations, the dominant fragmentation mechanism is, indeed, random successive evaporation of C_2 units. Nevertheless, very different fragmentation patterns were observed in experiments investigating *negative* ion spectra obtained from fullerene fragmentations.[31–34] Very few negatively charged fullerene fragments are detected, this being attributed to the very high probability of thermal electron emission leading to only neutral fragments (that go undetected).

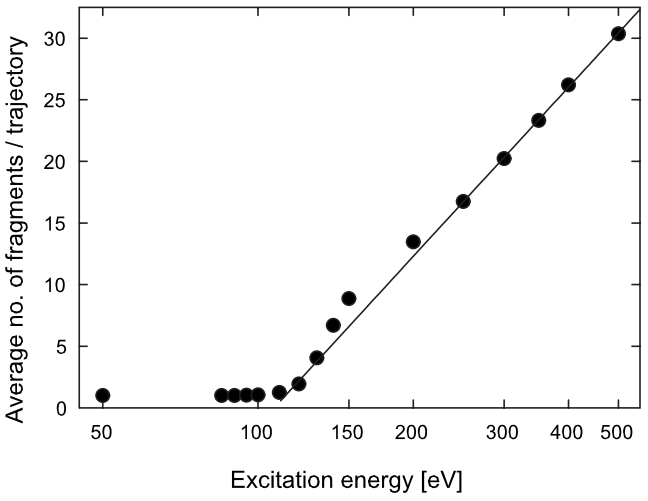

FIG. 7. Average number of fragments per trajectory vs excitation energy (semilogarithmic plot).

As the excitation energy increases, there is increasing probability for the emission of larger neutral fragments (C_4 or C_6). Provided the excitation energy is sufficiently large, the initial fragmentation process can lead to a complete disintegration of the fullerene cage. Multiple large fragments result, which can subsequently undergo C_2 or (predominantly) metastable C_3 loss. This scenario is supported by some molecular dynamics simulations[10,11,35,36] and has been proven explicitly for photodissociation experiments using nanosecond laser pulses.[37,38] Experimentally, the detection of large neutral fragments from collision experiments, under conditions where the positively charged fragments show a bimodal distribution, was reported by McHale *et al.*[39] A mass distribution closely mirroring that of the positively charged fragments was obtained and provided evidence in favor of a cleavage mechanism producing large neutral fragments at collision energies of 340 eV, rather than the dominance of successive C_2 emission.

Another relevant quantity derived from our simulations is the average number of fragments per trajectory, $\langle N_{\mathrm{frag}} \rangle$. This was computed as ensemble-cumulated number of fragments divided by the number of trajectories for a given excitation energy. Alternatively, it can be obtained as the inverse of the average fragment size. The semilogarithmic plot in Fig. 7

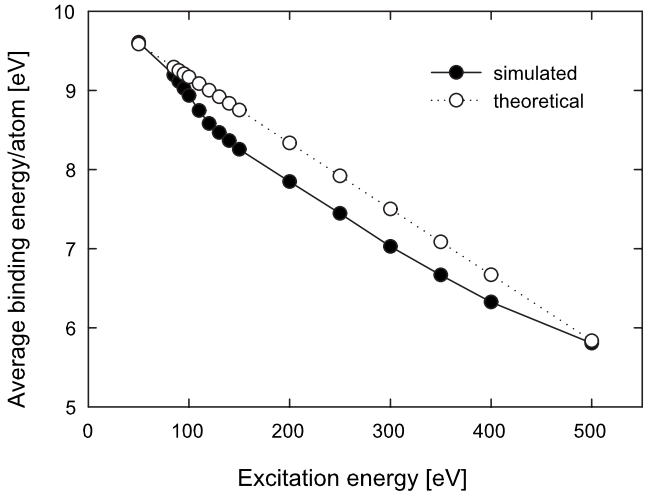

FIG. 8. Simulated and theoretical average binding energy per atom vs excitation energy. The slightly lower simulated values are responsible for the nonfragmenting deformations of the fullerene.

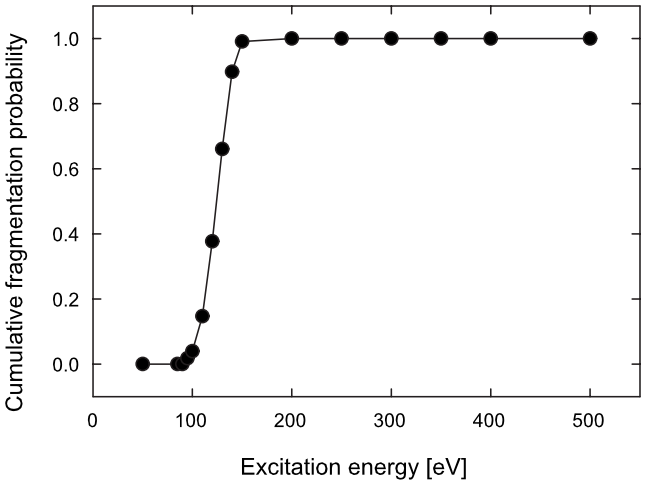

FIG. 9. The cumulative fragmentation probability shows a phase transition in the 100–120 eV excitation energy range.

allows for the activation energy of the C_{60} fragmentation to be readily obtained from the intercept of the linear model:

$$\langle N_{\text{frag}} \rangle = \alpha \ln E + \beta.$$

The optimized parameters are $\alpha = 19.80$ and $\beta = -92.61$ and, correspondingly, the activation energy $E_a = 113$ eV is found. This value is well situated in the interval of 80–225 eV determined by Rentenier *et al.* for the activation of the fullerene fragmentation subject to proton impact.[4] In the same interval, irrespective of the projectile species but depending on the particular charge, also a relatively sharp phase transition was found (see Fig. 3 of Rentenier *et al.*).

The average binding energy per atom is obtained by averaging the final total binding energy per atom over the whole trajectory ensemble for each given energy. In the employed TB parametrization, the initial binding energy for a carbon atom in the C_{60} cage is 10.00 eV, in fairly good agreement with the value of 9.55 eV obtained from DFT calculations based on the PBE exchange-correlation functional of Perdew *et al.*[40] and the 6-31G(d) basis set.

The dependence of the average binding energy *at the end* of the trajectories on the excitation energy is compared in Fig. 8 with theoretical reference values calculated simply as differences between the binding energy at 0 K and the excitation energies per atom. Obviously, the simulations slightly underestimate the corresponding linearly decreasing reference values and this is due to the deformation energy stored in the various fragments, which is not being taken into account in the simple reference model. Still, the simulated curve features a noticeable inflection in the phase transition region (100–120 eV).

For small excitation energies, only a fraction of the total number of simulated trajectories results in dissociated fullerenes. The cumulative fragmentation probability, defined as total number of dissociated cages divided by the total number of trajectories, is depicted in Fig. 9 and clearly shows the phase transition in the energy range of 100–120 eV. For energies above 150 eV, all C_{60} cages undergo at least one dissociation process, the cumulative fragmentation probability amounting to 1.

V. CONCLUSIONS

The radiation-induced fragmentation of the C_{60} fullerene was investigated in the excitation energy range of 50–500 eV by means of tight-binding molecular dynamics simulations based on the parametrization of Papaconstantopoulos *et al.*[1] For each considered excitation energy, all calculated distributions were averaged over an ensemble of 200 trajectories, with random initial atomic velocities assigned to the equilibrium structure of C_{60}. The general findings are similar to those obtained in several time-of-flight experiments,[2,4,5,17] confirming for relatively low excitation energies (<150 eV) the U shape of the fragment size distributions and the fact that the commonly accepted power-law behavior for small fragment sizes does not set in for energies up to 500 eV.

For each excitation energy, fragment size distributions, average fragment sizes, average and overall minimum (maximum) fragment sizes, binding energies, and relative and/or cumulative fragmentation probabilities were calculated. For small fragments and excitation energies above 400 eV, a tendency of the size distributions to transform into power laws becomes apparent. For high excitation energies, multifragmentation turns out to be the main fragmentation channel, while for low energies, evaporation of small clusters plays a decisive role.

For low excitation energies, the small fragment distributions are peaked at the dimers or trimers, rather than at the monomer. Fragments with high even number of atoms (>50) are more likely to occur than odd size fragments, the primary fragmentation channel being the sequential loss of neutral dimers. This bimodal size dependence characterizes

both the distributions of the small and large fragments. In the intermediate energy range (150–350 eV), the main fragmentation channel found was the loss of trimers, which appear to be, along with the dimers, the most stable fragments.

In the 100–120 eV energy interval, a phase transition develops, in fair agreement with the results of the experiments mentioned above and with similar tight-binding molecular dynamics simulations.[9–12]

*tbeu@phys.ubbcluj.ro

[1] D. A. Papaconstantopoulos, M. J. Mehl, S. C. Erwin, and M. R. Pederson, MRS Symposia Proceedings No. 491 (Materials Research Society, Pittsburgh, 1998), p. 221.
[2] E. B. Campbell and F. Rohmund, Rep. Prog. Phys. **63**, 1061 (2000).
[3] V. V. Afrosimov, A. A. Basalaev, M. N. Panov, and O. V. Smirnov, Fullerenes, Nanotubes, Carbon Nanostruct. **12**, 485 (2004).
[4] A. Rentenier, P. Moretto-Capelle, D. Bordenave-Montesquieu, and A. Bordenave-Montesquieu, J. Phys. B **38**, 789 (2005).
[5] D. M. Gruen, Nucl. Instrum. Methods Phys. Res. B **78**, 118 (1993).
[6] S. C. O'Brien, J. R. Heat, R. F. Curl, and R. E. Smalley, J. Chem. Phys. **88**, 220 (1988).
[7] W. A. Harrison, *Solid State Theory* (McGraw-Hill, New York, 1970).
[8] W. A. Harrison, *Electronic Structure and the Properties of Solids* (W. H. Freeman & Co., San Francisco, 1980).
[9] C. Z. Wang, C. H. Xu, C. T. Chan, and K. M. Ho, J. Phys. Chem. **96**, 3563 (1992).
[10] E. Kim, Y. H. Lee, and J. Y. Lee, Phys. Rev. B **48**, 18230 (1993).
[11] S. G. Kim and D. Tomanek, Phys. Rev. Lett. **72**, 2418 (1994).
[12] B. Torralva, T. A. Niehaus, M. Elstner, S. Suhai, Th. Frauenheim, and R. E. Allen, Phys. Rev. B **64**, 153105 (2001).
[13] T. A. Beu, J. Onoe, and K. Takeuchi, Eur. Phys. J. D **10**, 391 (2000).
[14] T. A. Beu, J. Onoe, and K. Takeuchi, Eur. Phys. J. D **17**, 205 (2001).
[15] T. A. Beu, J. Onoe, and A. Hida, Phys. Rev. B **72**, 155416 (2005).
[16] T. A. Beu and J. Onoe, Phys. Rev. B **74**, 195426 (2006).
[17] Th. Frauenheim, G. Seifert, and M. Elstner, Phys. Status Solidi B **217**, 41 (2000).
[18] P. Hohenberg and W. Kohn, Phys. Rev. **136**, B864 (1964).
[19] J. C. Slater and G. F. Koster, Phys. Rev. **94**, 1498 (1954).
[20] C. S. Yannoni, P. P. Bernier, D. S. Bethune, G. Meijer, and J. R. Salem, J. Am. Chem. Soc. **113**, 3190 (1991).
[21] Q. M. Zhang, J.-Y. Yi, and J. Bernholc, Phys. Rev. Lett. **66**, 2633 (1991).
[22] E. E. B. Campbell, K. Hoffmann, H. Rottke, and I. V. Hertel, J. Chem. Phys. **114**, 1716 (2001).
[23] M. Tchaplyguine, K. Hoffmann, O. Duhr, H. Hohmann, G. Korn, H. Rottke, M. Wittmann, I. V. Hertel, and E. E. B. Campbell, J. Chem. Phys. **112**, 2781 (1999).
[24] A. Itoh, H. Tsuchida, K. Miyabe, T. Majima, and Y. Nakai, Phys. Rev. A **64**, 032702 (2001).
[25] T. LeBrun, H. G. Berry, S. Cheng, R. W. Dunford, H. Esbensen, D. S. Gemmell, E. P. Kanter, and W. Bauer, Phys. Rev. Lett. **72**, 3965 (1994).
[26] T. Schlathölter, R. Hoekstra, and R. Morgenstern, J. Phys. B **31**, 1321 (1998).
[27] A. Itoh and H. Tsuchida, Nucl. Instrum. Methods Phys. Res. B **195**, 216 (2002).
[28] W. Bauer, Nucl. Phys. A **681**, 441c (2001).
[29] R. Ehlich, M. Westerburg, and E. E. B. Campbell, J. Chem. Phys. **104**, 1900 (1996).
[30] Y. Cui and L. Liu, Phys. Rev. B **56**, 3624 (1997).
[31] D. Mathur, C. Brink, P. Hvelplund, N. Jensen, and D. H. Yu, Rapid Commun. Mass Spectrom. **9**, 114 (1994).
[32] H. Shen, C. Brink, P. Hvelplund, and M. O. Larsson, Z. Phys. D: At., Mol. Clusters **40**, 371 (1996).
[33] A. B. Young, L. M. Cousins, and A. G. Harrison, Rapid Commun. Mass Spectrom. **5**, 226 (1991).
[34] D. H. Yu, L. H. Andersen, C. Brink, P. Hvelplund, D. C. Lorents, and R. Ruoff, Mol. Mater. **4**, 237 (1994).
[35] L. Liu, K. Chen, and Y. Li, Chin. Phys. Lett. **10**, 720 (1993).
[36] Y. Xia, Y. Xing, C. Tan, and L. Mei, Phys. Rev. B **52**, 110 (1995).
[37] H. Hohmann, R. Ehlich, S. Furrer, O. Kittelmann, J. Ringling, and E. E. B. Campbell, Z. Phys. D: At., Mol. Clusters **33**, 143 (1995).
[38] K. R. Lykke, Phys. Rev. A **52**, 1354 (1995).
[39] K. J. McHale, M. J. Polce, and C. Wesdemiotis, J. Mass Spectrom. **30**, 33 (1995).
[40] J. P. Perdew, K. Burke, and M. Ernzerhof, Phys. Rev. Lett. **77**, 3865 (1996).